

Article

# Comparison of Precipitation Rates from Global Datasets for the Five-Year Period from 2019 to 2023

Heike Hartmann 

Department of Chemistry and Environmental Geosciences, Slippery Rock University of Pennsylvania, Slippery Rock, PA 16057, USA; heike.hartmann@sru.edu; Tel.: +1-724-738-4376

**Abstract:** Precipitation is a fundamental component of the hydrologic cycle and is an extremely important variable in meteorological, climatological, and hydrological studies. Reliable climate information including accurate precipitation data is essential for identifying precipitation trends and variability as well as applying hydrologic models for purposes such as estimating (surface) water availability and predicting flooding. In this study, I compared precipitation rates from five reanalysis datasets and one analysis dataset—the European Centre for Medium-Range Weather Forecasts Reanalysis Version 5 (ERA-5), the Japanese 55-Year Reanalysis (JRA-55), the Modern-Era Retrospective Analysis for Research and Applications Version 2 (MERRA-2), the National Center for Environmental Prediction/National Center for Atmospheric Research Reanalysis 1 (NCEP/NCAR R1), the NCEP/Department of Energy Reanalysis 2 (NCEP/DOE R2), and the NCEP/Climate Forecast System Version 2 (NCEP/CFSv2)—with the merged satellite and rain gauge dataset from the Global Precipitation Climatology Project in Version 2.3 (GPCPv2.3). The latter was taken as a reference due to its global availability including the oceans. Monthly mean precipitation rates of the most recent five-year period from 2019 to 2023 were chosen for this comparison, which included calculating differences, percentage errors, Spearman correlation coefficients, and root mean square errors (RMSEs). ERA-5 showed the highest agreement with the reference dataset with the lowest mean and maximum percentage errors, the highest mean correlation, and the smallest mean RMSE. The highest mean and maximum percentage errors as well as the lowest correlations were observed between NCEP/NCAR R1 and GPCPv2.3. NCEP/DOE R2 showed significantly higher precipitation rates than the reference dataset (only JRA-55 precipitation rates were higher), the second lowest correlations, and the highest mean RMSE.



Academic Editor: Andrzej Walega

Received: 7 December 2024

Revised: 28 December 2024

Accepted: 30 December 2024

Published: 1 January 2025

**Citation:** Hartmann, H. Comparison of Precipitation Rates from Global Datasets for the Five-Year Period from 2019 to 2023. *Hydrology* **2025**, *12*, 4. <https://doi.org/10.3390/hydrology12010004>

**Copyright:** © 2025 by the author. Licensee MDPI, Basel, Switzerland. This article is an open access article distributed under the terms and conditions of the Creative Commons Attribution (CC BY) license (<https://creativecommons.org/licenses/by/4.0/>).

**Keywords:** precipitation; reanalysis datasets; merged satellite and rain gauge dataset; global

## 1. Introduction

Access to reliable and high-quality climate information is essential in coping with current and future climate variability and change [1]. The availability of accurate precipitation data is of fundamental importance for applying hydrologic models for purposes such as water resource management, irrigation planning, hydropower operations, and forecasting of floods and droughts [2]. Accurate precipitation data are also needed for calibrating remote sensing products [3] and climate models [4] to facilitate future projections.

Particularly in high mountainous regions, climate information is often highly uncertain. The complex terrain and orographic effects cause high spatiotemporal variability in precipitation [5,6] which is often not captured by the comparatively few climate stations.

For example, in the Tarim River basin in northwestern China, climate stations are predominantly located in the lowlands and in the valleys of the mountains, where access is easy; very few stations are present at higher elevations [7,8]. Scarcity of climate data has also been reported from the Asian Himalayas [9–11] and the Tibetan Plateau [12,13] and from the South American Andes [6,14], the African Atlas mountains [15,16] and the Ethiopian highlands [17].

Particularly in regions where in situ ground observations are scarce, reanalysis data often seem to be the best option. Global reanalysis datasets are globally complete and are therefore sometimes referred to as “maps without gaps” [18,19]. After previous research in the 1980s [20,21], concentrated efforts have been made to generate multi-year global reanalyses since the early 1990s [22,23]. A retrospective analysis, also known as reanalysis, is produced via a frozen data assimilation system and numerical weather prediction model [24] that, by ingesting available observations, achieves hindcasting [25]. The goal of a climate reanalysis is to generate consistent and accurate climate datasets for a longer period.

Global reanalyses not only provide global spatial coverage; they also do not have gaps in time series. However, the reliability of the reanalysis data varies in time and space. If no in situ observations are available for a region, the quality of the reanalysis will be reduced, especially in that region. In situations where observations are missing, the reanalysis relies on imperfect information; therefore, as reanalysis data are available for regions where ground observational data are scarce, their limitations should be known and accounted for [26].

Another reason that reanalysis data are attractive is the enormous number of atmospheric variables available. The first global atmospheric reanalysis provided by U.S. agencies, the National Center for Environmental Prediction/National Center for Atmospheric Research Reanalysis 1 (NCEP/NCAR R1), already offered numerous atmospheric variables on multiple vertical levels. In addition to air temperature and geopotential height at 17 levels, many other variables such as relative humidity of the total atmospheric column, runoff, potential evaporation rate, water equivalent of accumulated snow depth, and precipitation rate were provided; some of these variables, such as air temperature and geopotential height, were designated as type A variables in NCEP/NCAR R1, indicating the most reliable class that is strongly influenced by observed data [22]. Precipitation rate was classified as a type C variable that is completely determined by the model [22] and thus should be used with caution [27]. In some of the more modern reanalyses, for example, in MERRA-2, precipitation observations are used in the assimilation process [28,29], possibly making precipitation rates more realistic.

One of the difficulties in working with reanalysis data is that the accuracy of reanalysis results is less well understood compared to the accuracy of observations [30]. Given the large number of reanalysis projects, it is challenging to find the most appropriate reanalysis with which to answer a research question, as there is uncertainty in any given reanalysis.

How large are the spatiotemporal differences between precipitation rates from reanalysis datasets and a precipitation dataset that is based on in situ observations and information from satellites? To allow for a more educated choice in the usage of precipitation data, especially in areas where in situ observational data are sparse, this paper compares precipitation rates from five reanalysis datasets and one analysis dataset with precipitation data from a merged satellite and rain gauge dataset.

## 2. Materials and Methods

### 2.1. Materials

In this study, precipitation rates from the European Centre for Medium-Range Weather Forecasts Reanalysis Version 5 (ERA-5), the Japanese 55-Year Reanalysis (JRA-55), the Modern-Era Retrospective Analysis for Research and Applications Version 2 (MERRA-2), the NCEP/NCAR R1, the NCEP/Department of Energy Reanalysis 2 (NCEP/DOE R2), and the NCEP/Climate Forecast System Version 2 (NCEP/CFsv2) were compared with precipitation data from the merged satellite and rain gauge dataset from the Global Precipitation Climatology Project in Version 2.3 (GPCPv2.3) over the most recent five year period from 2019 to 2023. All datasets provide precipitation rates globally and include the oceans. This was also the main reason for choosing GPCPv2.3 as the reference dataset over other precipitation datasets. General information about all datasets is summarized in Table 1. The following subchapters provide more detailed information about each dataset.

#### 2.1.1. ERA-5

ERA-5 is the newest reanalysis conducted by ECMWF within the Copernicus Climate Change Service (C3S) and replaced the ERA-Interim reanalysis. Hersbach et al. [19] provided a comparison of ERA-5 with ERA-Interim as well as details of the ERA-5 global reanalysis. Additional information was taken from the ERA-5 data documentation [31]. ERA5 is produced using four-dimensional variational (4D-Var) data assimilation and model forecasts in the Integrated Forecasting System (IFS) Cy41r2, which has been used operationally since 2016. From the surface up to 0.01 hPa, the atmosphere is resolved using 137 levels. The atmospheric model in the IFS is coupled to a land surface model and an ocean wave model [31]. Information on precipitation stems mostly from satellite observations; however, ERA5 uses information on rain rate from ground-based radar–gauge composite observations, produced since 2009, in addition [19]. In ERA-5, total precipitation is provided in meters of water equivalent. The precipitation data [32] were downloaded from the Copernicus Climate Change Service (C3S) Climate Data Store (CDS) in their native units and were subsequently converted to [mm/day]. A summary of the ERA5 atmospheric reanalysis was given by Hersbach et al. [33].

#### 2.1.2. JRA-55

JRA-55 is the second Japanese global reanalysis provided by the Japan Meteorological Agency (JMA) and followed JRA-25. Kobayashi et al. [34] and Harada et al. [35] provided details about JRA-55 as well as a comparison with JRA-25. From December 2009 to January 2024, JRA-55 was produced using the TL319 version of the JMA operational 4D-Var data assimilation system. From the surface up to 0.1 hPa, the atmosphere was resolved in 60 levels. In addition to observations used in ERA-40 and those archived by JMA, JRA-55 also incorporated reprocessed satellite data from major meteorological satellite centers as well as several observational datasets, including homogenized radiosonde temperature observations [34]. However, rain gauge data were not used in the assimilation process, and total precipitation was considered a two-dimensional average diagnostic field [36]. Total precipitation provided in [mm/day] was downloaded from the NCAR Computational and Information Systems Laboratory [37]. A summary of the dataset was given by Kobayashi et al. [38].

#### 2.1.3. MERRA-2

MERRA-2, the successor of MERRA, is the most recent atmospheric reanalysis produced by NASA's Global Modeling and Assimilation Office (GMAO). Gelaro et al. [28] provided details about the reanalysis. For MERRA-2, an updated version of the God-

standard Earth Observing System (GEOS), the GEOS-5 atmospheric general circulation model, was developed [39]. MERRA-2 is produced using 3D-Var data assimilation and is the first reanalysis to assimilate aerosol observations [28]. From the surface up to 0.01 hPA, the atmosphere is partitioned into 72 levels [28]. MERRA-2 corrects the model-generated precipitation with precipitation observations before reaching the land surface [29]. In MERRA-2, total precipitation is provided in  $[\text{kg}/(\text{m}^2\text{s})]$ . Precipitation data from MERRA-2 [40] were downloaded in their native units via the Climate Explorer [41] and were then converted to  $[\text{mm}/\text{day}]$ . An outline of the NASA's MERRA-2 reanalysis was given by Bosilovich et al. [42].

#### 2.1.4. NCEP/NCAR R1

The NCEP and NCAR have been cooperating on the NCEP/NCAR Reanalysis 1 since 1991 [22]. It is the first global atmospheric reanalysis provided by U.S. agencies that was initially planned to cover 40 years from 1957 to 1996 [22] and was then extended backwards to 1948 [27]. NCEP/NCAR R1 uses a frozen state-of-the-art global data assimilation system [27] and is updated until today. The following information on the dataset was taken from Kalnay et al. [22]. NCEP/NCAR R1 is produced using 3D-Var data assimilation and assimilates rawinsonde observations; surface marine data from ships, buoys, and ocean stations; aircraft data; land synoptic data; and satellite information. From the surface up to 2.7 hPA, the atmosphere is resolved using 28 levels. The frozen climate data assimilation system allows researchers to evaluate whether current climate anomalies are significant when compared to a long reanalysis with an unchanged data assimilation system. In NCEP/NCAR R1, precipitation is considered a Type C variable that is completely determined by the model.

Today, due to the frozen data assimilation system, the resolution of NCEP/NCAR R1 lags behind the more modern reanalyses. In NCEP/NCAR R1, precipitation rates are provided in  $[\text{kg}/(\text{m}^2\text{s})]$ . Precipitation rates from NCEP/NCAR R1 were retrieved from the website of the Physical Sciences Laboratory (PSL) of the National Oceanic and Atmospheric Administration (NOAA) [43]. They were downloaded in their native units and were subsequently converted to  $[\text{mm}/\text{day}]$ .

#### 2.1.5. NCEP/DOE R2

After the main production phase of NCEP/NCAR R1, several human processing errors were discovered that could not be fixed anymore at the time they were found, and therefore another reanalysis project, NCEP/DOE R2, was started in 1998 [44]. Details of NCEP/DOE R2 were provided in Kanamitsu et al. [44], and the brief description of the dataset provided here is based on this publication. In addition to fixing the human processing errors present in NCEP/NCAR R1, the forecast model and data assimilation system in NCEP/DOE R2 were upgraded, and a diagnostic package was developed. The 3D-Var data assimilation process and the spatial and temporal resolutions were kept. The raw observational data used in the assimilation process are similar to NCEP/NCAR R1. However, in NCEP/DOE R2, observed 5-day mean "pentad" precipitation values, based on a global precipitation analysis that merged satellite and gauge measurements [45], was implemented as forcing. The period covered by NCEP/DOE R2 extends back only until 1979 and is restricted to the satellite period. NCEP/DOE R2 is an upgraded and human-error-fixed version of NCEP/NCAR R1 but not a next-generation reanalysis. Therefore, the resolution of NCEP/DOE R2 lags behind the more modern reanalyses as well. As in NCEP/NCAR R1, precipitation rates in NCEP/DOE R2 are provided in  $[\text{kg}/(\text{m}^2\text{s})]$ . Precipitation rates from NCEP/DOE R2 were retrieved from the website of the NOAA PSL [46]. They were downloaded in their native units and then converted to  $[\text{mm}/\text{day}]$ .

### 2.1.6. NCEP/CFSv2

NCEPs' CFSv2 is the second version of the NCEP Climate Forecast System and has been used operationally since March 2011 [47]. Saha et al. [47] described NCEP/CFSv2 in detail, and the outline given here is based on this publication. Some differences from the first Climate Forecast System (CFSv1) are its upgraded four-level soil model, an interactive three-layer sea ice model, and rising CO<sub>2</sub> concentrations. Even though the ocean and sea ice models are identical to those used in the Climate Forecast System Reanalysis (CFSR) [48], the atmospheric and the land surface components are slightly different. The differences lie mainly in the physical parameterization of the atmospheric model and some tuning parameters in the land surface model. As in CFSv1, the atmosphere is vertically resolved in 64 levels [49], from the surface up to 0.266 hPA [48]. So far, all of NCEPs CFS products have been produced using 3D-Var data assimilation [50]. In CFSv2, observed precipitation is used as forcing for the land model [51]. Total precipitation in NCEP/CFSv2 is provided in [kg/(m<sup>2</sup>s)]. Precipitation data from NCEP/CFSv2 were downloaded from the NCAR Research Data Archive [52] in their native units and were subsequently converted to [mm/day].

### 2.1.7. GPCPv2.3

The GPCP was established as part of the Global Energy and Water Cycle Exchanges (GEWEX) activity under the World Climate Research Program (WCRP) in 1986 [53]. The mission of the GPCP has been to produce global analyses of area- and time-averaged precipitation data to be used in climate research [54]. Over the years, techniques were developed to combine precipitation estimates from satellite data and precipitation gauge observations [53,55], and the GPCP Version 1 Combined Precipitation Data Set was released in 1996. Traditionally, the GPCP precipitation datasets merge satellite-based estimates over ocean and land with the precipitation gauge analyses over land from the Global Precipitation Climatology Centre (GPCC) in Germany [53,55,56]. The GPCPv2.3 became available in 2016 [57]. Passive microwave-based (PMW) rainfall estimates from the Special Sensor Microwave/Imager (SSM/I) and the Special Sensor Microwave Imager Sounder (SSMIS), infrared rainfall estimates from a series of geostationary and polar-orbiting satellites, and observations from surface rain gauges from the GPCC are used in this product [58]. More details about the dataset were provided in Adler et al. [56]. Average monthly rates of precipitation from GPCPv2.3 were downloaded in [mm/day] from the website of the NOAA PSL [59].

**Table 1.** Overview of the datasets used for monthly precipitation data.

Dataset	Abbreviation	Highest Spatial Resolution (lat × lon)	Time Period, Highest Temporal Resolution	Source
European Centre for Medium-Range Weather Forecasts Reanalysis version 5	ERA-5	0.25° × 0.25°	1940–now, hourly	Hersbach et al. [19] <a href="https://cds.climate.copernicus.eu/datasets/reanalysis-era5-single-levels-monthly-means">https://cds.climate.copernicus.eu/datasets/reanalysis-era5-single-levels-monthly-means</a> (accessed on 1 December 2024)

Table 1. Cont.

Dataset	Abbreviation	Highest Spatial Resolution (lat × lon)	Time Period, Highest Temporal Resolution	Source
Japanese 55-Year Reanalysis	JRA-55	1.25° × 1.25°	1958–2024, 3-hourly	Kobayashi et al. [34]; Harada et al. [35] <a href="https://rda.ucar.edu/datasets/d628001/">https://rda.ucar.edu/datasets/d628001/</a> (accessed on 1 December 2024)
Modern-Era Retrospective Analysis for Research and Applications version 2	MERRA-2	0.5° × 0.625°	1980–now, hourly	Gelaro et al. [28] <a href="https://disc.gsfc.nasa.gov/datasets/M2TMNXAER_5.12.4/summary">https://disc.gsfc.nasa.gov/datasets/M2TMNXAER_5.12.4/summary</a> (accessed on 1 December 2024)
National Center for Environmental Prediction/National Center for Atmospheric Research reanalysis 1	NCEP/NCAR R1	1.875° × 1.904128°	1948–now, 6-hourly	Kalnay et al. [22]; Kistler et al. [27] <a href="https://psl.noaa.gov/data/gridded/data.ncep.reanalysis.html">https://psl.noaa.gov/data/gridded/data.ncep.reanalysis.html</a> (accessed on 1 December 2024)
National Center for Environmental Prediction/Department of Energy Reanalysis 2	NCEP/DOE R2	1.875° × 1.904128°	1979–now, 6-hourly	Kanamitsu et al. [44] <a href="https://psl.noaa.gov/data/gridded/data.ncep.reanalysis2.html">https://psl.noaa.gov/data/gridded/data.ncep.reanalysis2.html</a> (accessed on 1 December 2024)
National Center for Environmental Prediction/Climate Forecast System Version 2	NCEP/CFSv2	0.204° × 0.205°	2011–now, monthly (based on 6-hourly)	Saha et al. [47] <a href="https://rda.ucar.edu/datasets/d094002">https://rda.ucar.edu/datasets/d094002</a> (accessed on 1 December 2024)
Global Precipitation Climatology Project version 2.3	GPCPv2.3	2.5° × 2.5°	1979–now, monthly	Adler et al. [56] <a href="https://psl.noaa.gov/data/gridded/data.gpcp.html">https://psl.noaa.gov/data/gridded/data.gpcp.html</a> (accessed on 1 December 2024)

## 2.2. Methods

### 2.2.1. Calculations with Mean Values

At the outset of research, mean values of all grid cell time series in the different datasets were calculated to produce one map for each dataset showing the mean precipitation rates for the period from 2019 to 2023. These data were then regridded to a 2.5° spatial resolution to allow for spatial comparisons with the reference dataset GPCPv2.3. Regridding was carried out with a box averaging method, where the area-weighted integral of all input grid boxes which intersect an output grid box is divided by the area of the output grid box [60]. To visualize the differences between the various datasets and GPCPv2.3, the mean values of GPCPv2.3 were subtracted from the mean values of all other datasets, and the differences were plotted in maps. It is crucial to consider that especially in arid

regions, small differences in precipitation can represent a large percentage or even exceed the total annual precipitation. Therefore, percentage errors between the different datasets and GPCPv2.3 were calculated and visualized in maps. To show the effect that the often small daily differences have on an annual scale, mean annual total global precipitation was calculated.

Histograms of each dataset were plotted to check for normal distribution. None of the datasets was normally distributed; all were heavily skewed towards low precipitation values. To account for this, it was decided to calculate spatial Spearman rank correlation coefficients between each dataset and GPCPv2.3. Moreover, the spatial root mean square errors (RMSEs) between all datasets and GPCPv2.3 were calculated. Details about the Spearman Rank Correlation Coefficient and the RMSE can be found in Lohninger [61] and Chai and Draxler [62], respectively.

### 2.2.2. Calculations with Monthly Values

After that, the datasets were used in monthly resolution. Again, the datasets were regridded to a  $2.5^\circ$  spatial resolution with the method described above. I randomly chose six grid points in all datasets (three over land and three over the ocean). These grid cell time series were tested for normal distribution by plotting and interpreting histograms. All datasets showed at least one time series that was not normally distributed and heavily skewed towards low precipitation values. Therefore, the decision was made to once again calculate Spearman rank correlation coefficients between each dataset and GPCPv2.3. Then, the RMSEs between all datasets in monthly resolution and GPCPv2.3 were calculated.

## 3. Results

### 3.1. Results from Calculations with Mean Values

Figure 1 shows the maps of mean precipitation rates for the period from 2019 to 2023 for the different datasets. All datasets show a belt of high precipitation rates at about  $5^\circ$  north of the equator. The precipitation belt is more pronounced over the ocean and with higher precipitation rates over the Pacific than over the Atlantic and especially over the Indian ocean basins. Over the Indian ocean basin and the western Pacific, there is a second band of high precipitation rates at about  $5$  to  $10^\circ$  south. In NCEP/NCAR R1, NCEP/DOE R2, and JRA-55, the two bands cover a wider latitudinal range than in the other datasets, with higher precipitation rates in NCEP/DOE R2 and JRA-55. Clear variations are evident in the precipitation rates over tropical continental regions, including the northern South American and the African continent as well as the Malay Archipelago. Differing precipitation rates can also be observed over high-mountain Asia.

Mean values, mean differences, and maximum differences are documented in Table 2. Looking at the mean values, it becomes clear that all of the precipitation datasets show higher mean precipitation rates than GPCPv2.3, with the highest mean precipitation rate in the JRA-55 dataset and the second highest in NCEP/DOE R2. Accordingly, the highest mean differences are also seen between JRA-55 and GPCPv2.3, and the second highest are observed between NCEP/DOE R2 and GPCPv2.3. By far the highest maximum difference, however, is found between MERRA-2 and GPCPv2.3, followed by the maximum difference between NCEP/DOE R2 and GPCPv2.3. The smallest mean and maximum differences can be observed between NCEP/NCAR R1 and GPCPv2.3, followed by the mean and maximum differences between ERA-5 and the reference dataset.

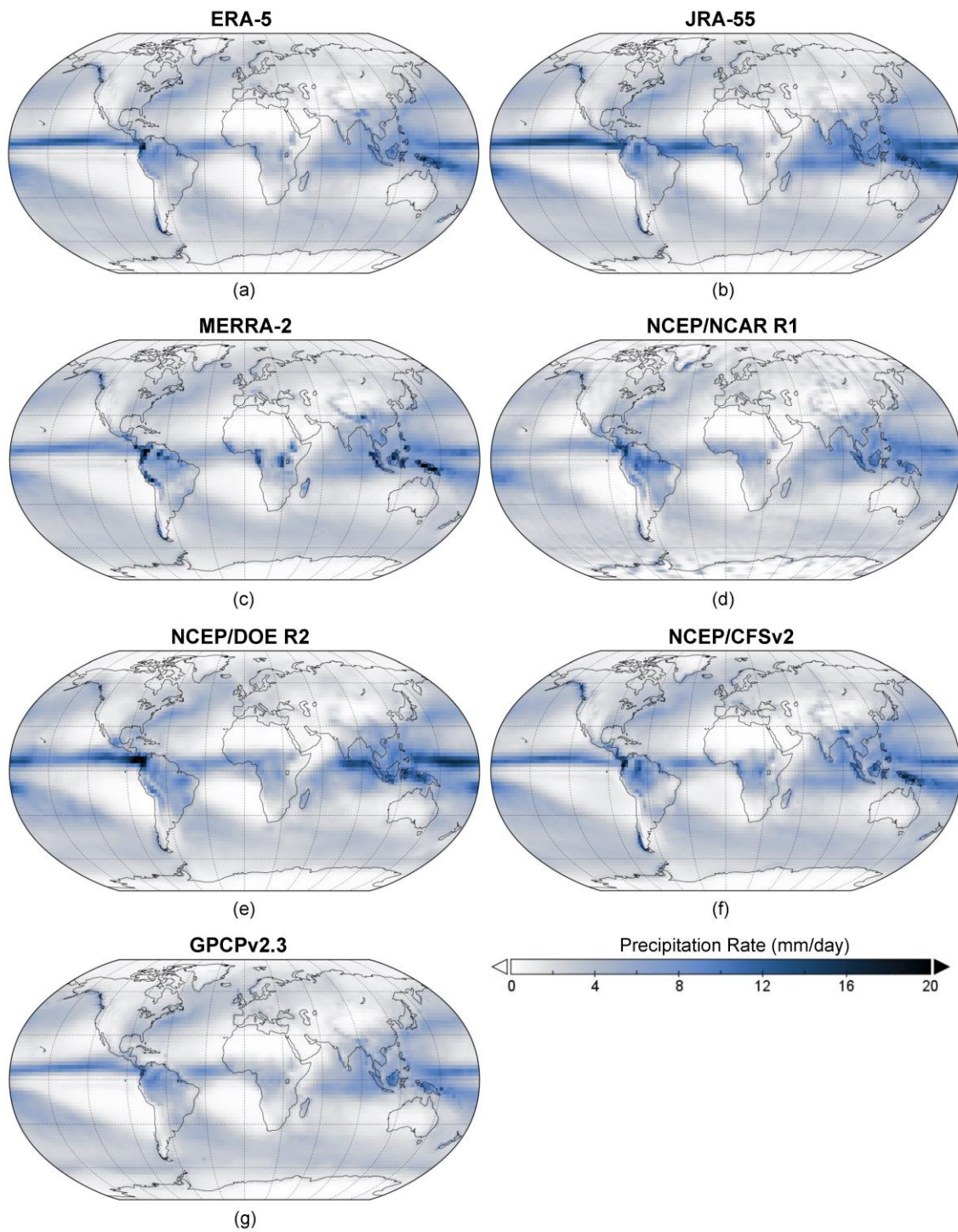


**Figure 1.** Mean precipitation rates for the period from 2019 to 2023 for the different datasets. Data are presented in a spatial resolution of  $2.5^\circ$ . The maps show mean precipitation rates from (a) ERA-5, (b) JRA-55, (c) MERRA-2, (d) NCEP/NCAR R1, (e) NCEP/DOE R2, (f) NCEP/CFSv2, and (g) GPCPv2.3.

**Table 2.** Area-weighted mean values [mm/day] of the different datasets that were previously regridded to a common  $2.5^\circ \times 2.5^\circ$  spatial resolution for the period from 2019 to 2023, their mean and maximum differences from GPCPv2.3 [mm/day], the mean and maximum percentage errors between all datasets and GPCPv2.3 [%], mean total global precipitation for all datasets, and the Spearman correlations coefficients (dimensionless) and root mean square errors (RMSEs) [mm/day] between all datasets and GPCPv2.3.

Precipitation Dataset	Mean [mm/day]	Mean Differences [mm/day]	Maximum Positive Differences [mm/day]	Mean Percentage Errors [%]	Maximum Percentage Errors [%]	Mean Total Global Precipitation [km <sup>3</sup> /year]	Spatial Spearman Correlation Coefficients	Spatial RMSEs [mm/day]
ERA-5	2.932	+0.264	9.701	28.9	521.1	~546,000	0.965	0.720
JRA-55	3.338	+0.670	7.822	37.6	913.6	~622,000	0.952	1.343
MERRA-2	2.964	+0.296	29.332	32.3	556.9	~552,000	0.959	1.176
NCEP/NCAR R1	2.800	+0.132	7.590	48.1	11,927.8	~522,000	0.870	1.165
NCEP/DOE R2	3.238	+0.570	12.224	40.6	525.3	~603,000	0.931	1.486
NCEP/CFSv2	3.205	+0.537	10.024	45.8	1,421.9	~597,000	0.955	0.981
GPCPv2.3	2.668	0	0	0	0	~497,000	1	0

Figure 2 spatially illustrates the differences between all datasets and the reference dataset GPCPv2. The perceived differences in the precipitation belts observed when looking at the mean precipitation rates before are now quantitatively expressed. In particular, JRA-55 and NCEP/DOE R2 show much higher precipitation rates over the ocean at  $5^\circ$  north compared to GPCPv2.3. ERA-5 and NCEP/CFSv2 depict slightly higher precipitation rates at  $5^\circ$  north than GPCPv2.3. MERRA-2 shows several grid cells in tropical regions over land with very high differences. Both the maximum difference of 29.332 mm/day and the second highest difference, 24.678 mm/day, can be found on New Guinea. A third very high difference, 24.114 mm/day, is observed over Colombia, with several adjacent cells over coastal northwestern South America showing high differences as well. Other areas showing higher precipitation in MERRA-2 compared to GPCPv2.3 include the Atlantic coast of Central Africa, the East African Rift Valley, the Himalayas, and the Tibetan Plateau, and generally the Malay Archipelago. However, over the ocean, the differences between MERRA-2 and GPCPv2.3 are comparatively small. At  $5^\circ$  north latitude, NCEP/NCAR R1 shows higher precipitation rates in the western Pacific but lower precipitation rates than GPCPv2.3 in the eastern tropical Pacific and in the Atlantic. Compared to GPCPv2.3, NCEP/DOE R2 depicts much higher precipitation values over southern Central America and the adjacent ocean area, as well as over the northern Indian Ocean basin and the Banda Sea. The grid cells with much lower precipitation rates than GPCPv2.3 can be detected east of New Guinea in both NCEP/NCAR R1 and NCEP/DOE R2. The highest difference between NCEP/CFSv2 and GPCPv2.3, 10.024 mm/day, is found off the southern west coast of South America. Other than that, the differences over the ocean are comparatively small. NCEP/CFSv2 shows a few grid cells over land with noticeably higher precipitation rates compared to GPCPv2.3. Over land, there are noticeably higher precipitation values in NCEP/CFSv2 over the Malay Archipelago, especially over New Guinea (9.405 mm/day) and south of the Himalayas (6.998 mm/day).

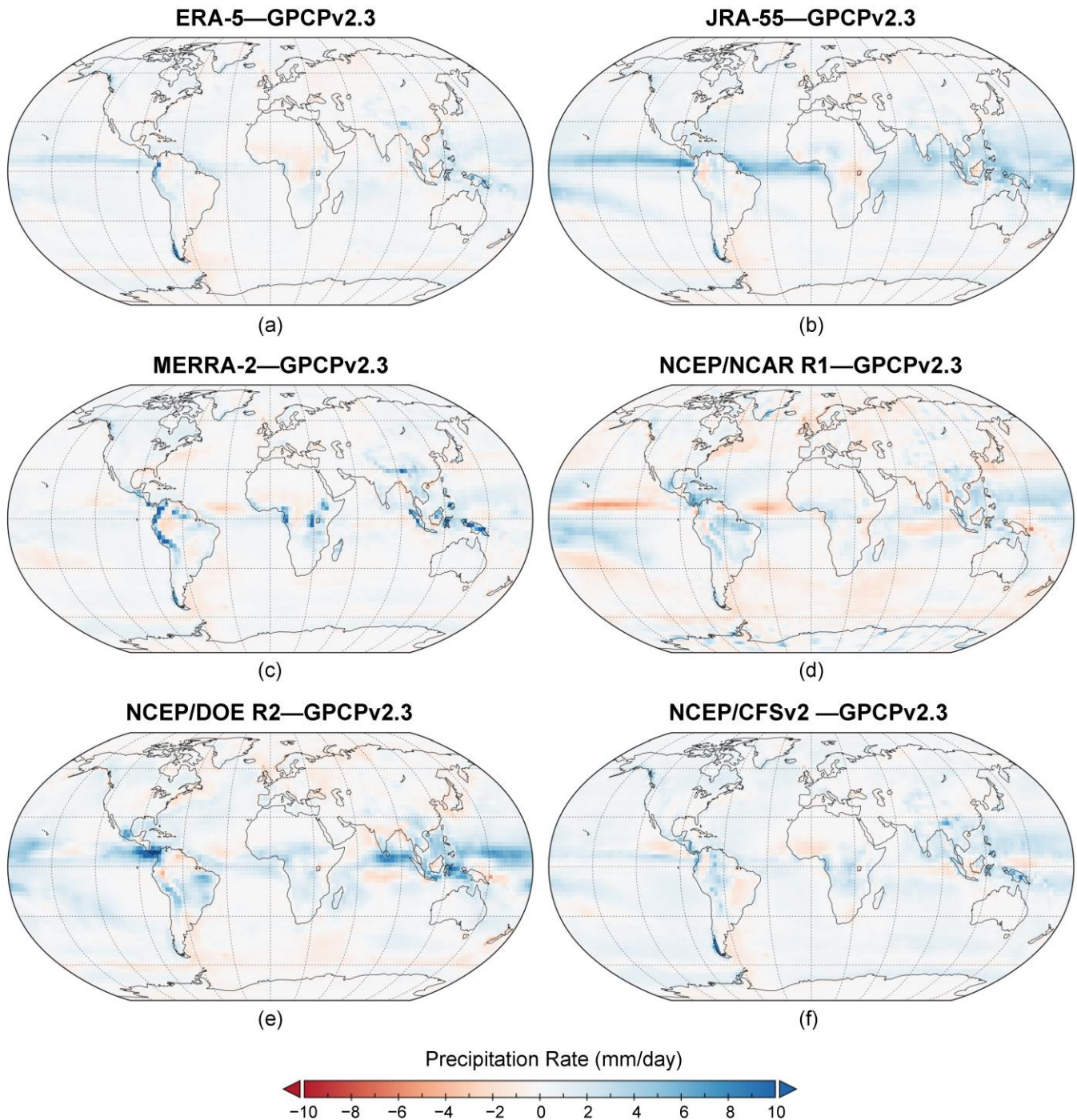


**Figure 2.** Differences between all datasets and the reference dataset for the period from 2019 to 2023. The maps show differences between precipitation rates from (a) ERA-5 and GPCPv2.3, (b) JRA-55 and GPCPv2.3, (c) MERRA-2 and GPCPv2.3, (d) NCEP/NCAR R1 and GPCPv2.3, (e) NCEP/DOE R2 and GPCPv2.3, and (f) NCEP/CFSv2 and GPCPv2.3.

The fact that larger differences in precipitation rates are not only observed in humid regions, but also in semi-arid regions such as the Tibetan Plateau, prompted the decision to calculate percentage errors. Looking at the mean and maximum percentage errors between the different precipitation datasets and the reference dataset in Table 2, ERA-5 shows—with 28.9% and 521.1%, respectively—the lowest percentage errors. The highest mean and by far the highest maximum percentage errors are detected between NCEP/NCAR R1 and the reference dataset. The mean percentage error between NCEP/NCAR R1 and GPCPv2.3

is 48.1% and the maximum percentage error, found over Antarctica, is 11,927.8%. The second highest mean and maximum percentage errors are observed between NCEP/CFSv2 and GPCPv2.3.

Figure 3 shows maps of percentage errors between all datasets and the reference dataset GPCPv2.3. All of the precipitation datasets show high percentage errors (>200%) over the Tibetan plateau and Central Asia and over western Greenland and Antarctica. Very high percentage errors (>400%) can be found over the oceanic regions with sparse precipitation along the west coasts of South America and/or southern Africa (>400%). In addition to the above-mentioned regions of high percentage errors, ERA-5 shows percentage errors between 40% and 120% over the Sahara desert and the Sahel, errors of up to 200% over the Atacama desert, and errors of >400% over southern Patagonia. In JRA-55, additional very high percentage errors of >400% can be observed over the Sahara, the Gulf of Aden, and southern Patagonia. MERRA-2 shows percentage errors > 400% over the Atacama desert and southern Patagonia. Percentage errors of 200% to up to 360% can be found over the East African Rift Valley and of up to 280% over New Guinea. By far the highest percentage errors are detected in NCEP/NCAR R1. Vast regions of Antarctica show percentage errors of >400%, which can also be observed over the Caribbean Sea, the coastal region of the Atacama desert, western Greenland, and Central Asia. The percentage errors between NCEP/DOE R2 and GPCPv2.3 are smaller compared to NCEP/NCAR R1 but still comparatively high and widespread. Areas with percentage errors > 400% are found over the Arabian Peninsula, the Sahara and the Atacama deserts, and over central Mexico. Even though the percentage errors between NCEP/CFSv2 and GPCPv2.3 over the oceanic regions along the west coasts of South America and southern Africa (>400%) are pronounced, grid cells with percentage errors > 400% are only found over Central Asia and over southern Patagonia. Over the Sahara desert and the Sahel, percentage errors are less than 120% and over the Atacama desert are up to 280%.

The column with mean annual total global precipitation in Table 2 visualizes the effect that the often small daily differences have on an annual scale. Over the course of a year, JRA-55 has a total of 125,000 km<sup>3</sup> precipitation more than GPCPv2.3; NCEP/DOE R2 has 106,000 km<sup>3</sup> excess precipitation. The two datasets with the smallest annual differences in precipitation, NCEP/NCAR R1 and ERA-5, still show excess precipitation of 25,000 km<sup>3</sup> and 49,000 km<sup>3</sup>, respectively.

The rest of the results from the calculations with mean values can also be taken from Table 2. The highest spatial Spearman rank correlation coefficient, 0.965, can be observed between GPCPv2.3 and ERA-5, followed by MERRA 2. The lowest spatial Spearman correlation coefficient, 0.87, is found between GPCPv2.3 and NCEP/NCAR R1, and the second lowest between GPCPv2.3 and NCEP/DOE R2. The lowest RMSE, 0.72 mm/day, is observed between ERA-5 and GPCPv2.3 and the highest, 1.486 mm/day, is between NCEP/DOE R2 and GPCPv2.3.

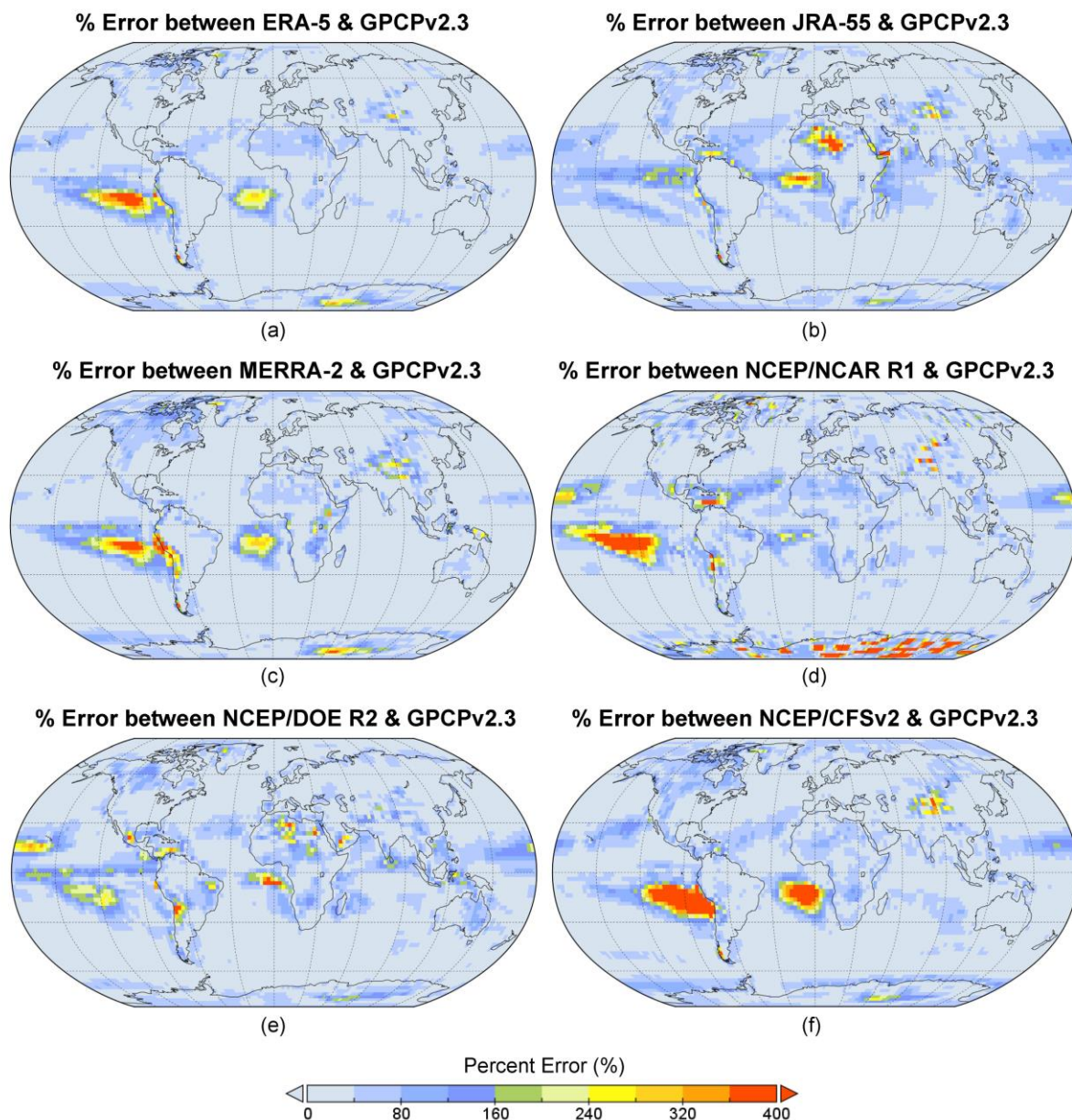


**Figure 3.** Percentage errors between all datasets and the reference dataset for the period from 2019 to 2023. The maps show percentage errors between precipitation rates from (a) ERA-5 and GPCPv2.3, (b) JRA-55 and GPCPv2.3, (c) MERRA-2 and GPCPv2.3, (d) NCEP/NCAR R1 and GPCPv2.3, (e) NCEP/DOE R2 and GPCPv2.3, and (f) NCEP/CFSv2 and GPCPv2.3.

### 3.2. Results from Calculations with Monthly Values

The Spearman rank correlation coefficients and the RMSEs between the different datasets and GPCPv2.3 in monthly resolution are spatially illustrated in maps; the correlation coefficients are depicted in Figure 4 and the RMSEs in Figure 5. Mean correlation coefficients, mean RMSEs, and maximum RMSEs are compiled in Table 3.

All maps depicting Spearman rank correlation coefficients show no correlation with the GPCPv2.3 dataset in regions with sparse precipitation, including the interior of Greenland and Alaska, the Sahara, and the Cape Horn region and to a lesser extent the Tibetan Plateau, the Gulf of Aden, and the oceanic region along the west coast of California. Areas with negative correlation that are present in all maps include the oceanic regions with sparse precipitation along the west coasts of South America and Southern Africa. All of the oceanic west coast regions are over cold ocean currents. MERRA-2 shows the largest areas

of negative correlation with GPCPv2.3, with the highest negative correlation coefficients being as low as  $-0.682$  on the west coast of southern Africa. Only NCEP/DOE R2 shows, with  $-0.698$ , a higher negative correlation coefficient. It is located on the west coast of South America. It is noticeable that compared to the other datasets, there are many more areas with no or only small correlation between NCEP/NCAR R1 and NCEP/DOE R2 and GPCPv2.3. It is also evident that both maps (Figure 3d) depict generally lower correlation coefficients than the other maps.

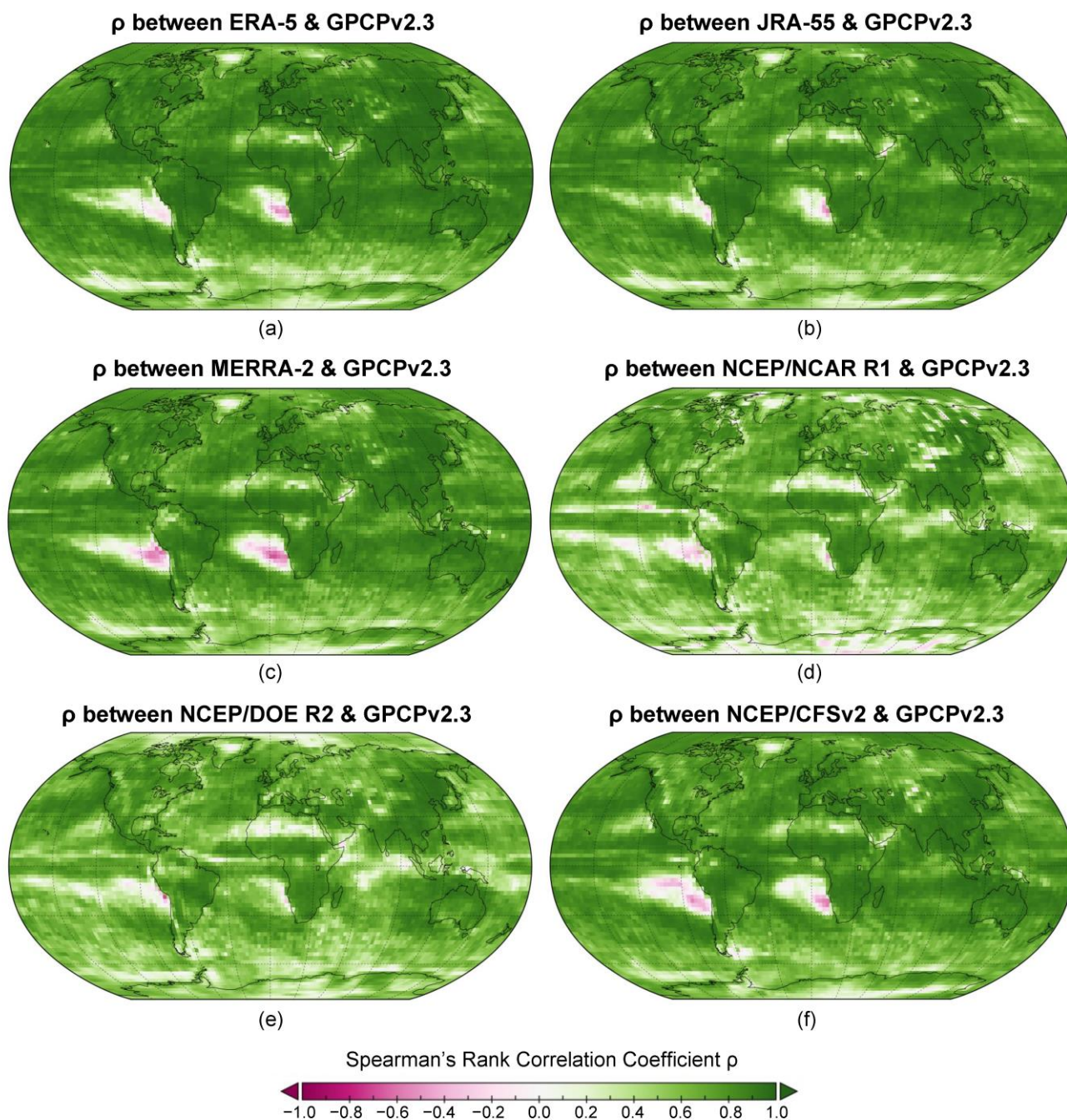


**Figure 4.** Spearman rank correlation coefficients between all datasets and the reference dataset in monthly resolution for the period from 2019 to 2023. The maps show Spearman rank correlation coefficients between (a) ERA-5 and GPCPv2.3, (b) JRA-55 and GPCPv2.3, (c) MERRA-2 and GPCPv2.3, (d) NCEP/NCAR R1 and GPCPv2.3, (e) NCEP/DOE R2 and GPCPv2.3, and (f) NCEP/CFSv2 and GPCPv2.3.

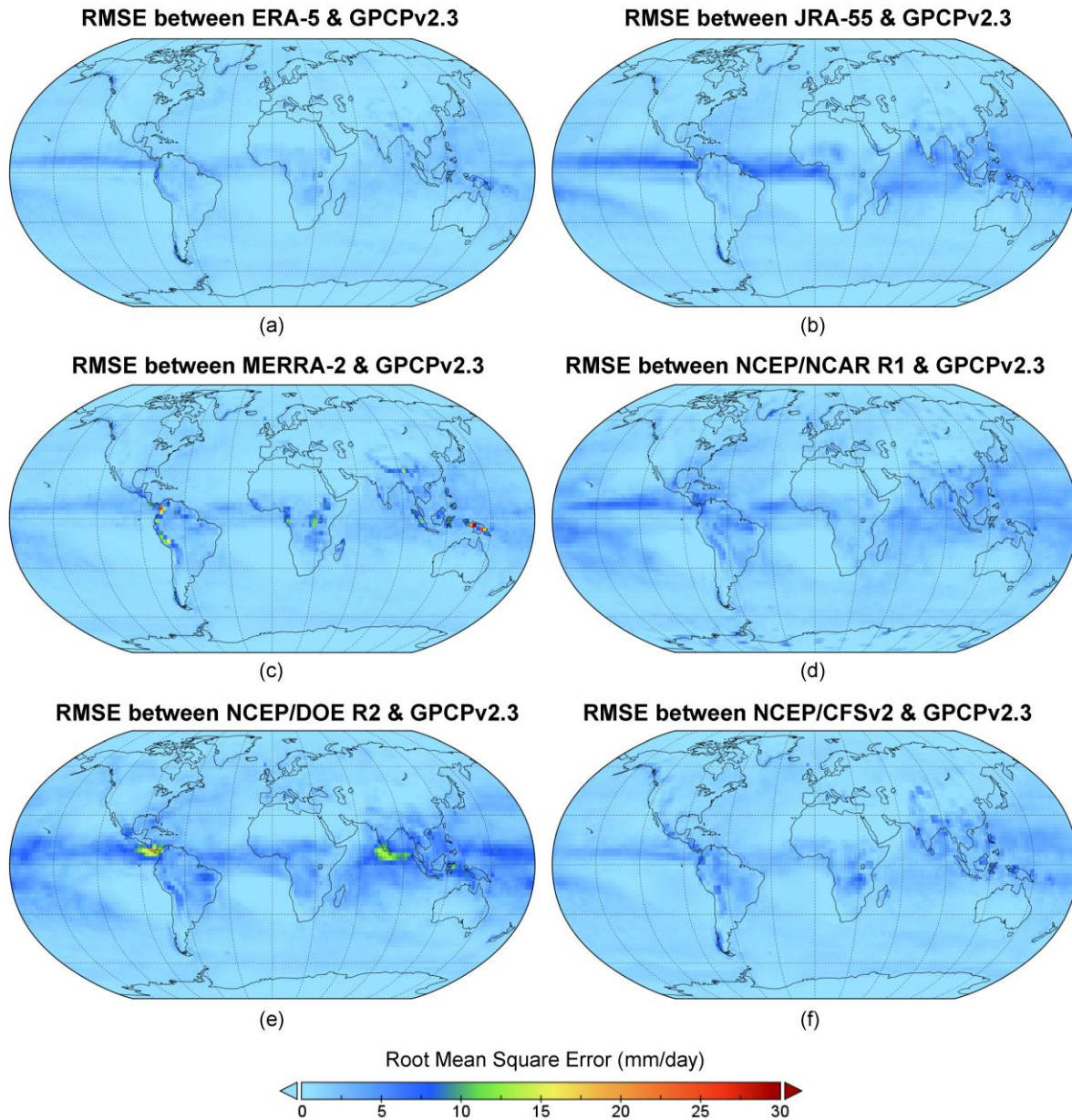


**Figure 5.** RMSEs between all datasets and the reference dataset in monthly resolution for the period from 2019 to 2023. The maps show RMSEs between (a) ERA-5 and GPCPv2.3, (b) JRA-55 and GPCPv2.3, (c) MERRA-2 and GPCPv2.3, (d) NCEP/NCAR R1 and GPCPv2.3, (e) NCEP/DOE R2 and GPCPv2.3, and (f) NCEP/CFSv2 and GPCPv2.3.

**Table 3.** Area-weighted mean Spearman correlation coefficients (dimensionless), root mean square errors (RMSEs) [mm/day], and maximum RMSEs [mm/day] between the different regridded datasets in monthly resolution and GPCPv2.3 for the period from 2019 to 2023.

Precipitation Dataset	Mean Spearman Correlation Coefficients	Mean RMSEs [mm/day]	Maximum RMSEs [mm/day]
ERA-5	0.787	1.036	10.097
JRA-55	0.776	1.420	9.142
MERRA-2	0.748	1.275	29.737
NCEP/NCAR R1	0.627	1.660	8.965
NCEP/DOE R2	0.633	2.016	16.862
NCEP/CFSv2	0.738	1.401	9.109
GPCPv2.3	1	0	0

The mean Spearman correlation coefficients support this observation. The lowest mean Spearman correlation coefficient, 0.627, can be observed between GPCPv2.3 and NCEP/NCAR R1, followed by NCEP/DOE R2 with a mean correlation coefficient of 0.633. The highest mean Spearman correlation coefficient, 0.787, can be found between GPCPv2.3 and ERA-5, and the second highest, 0.776, is between GPCPv2.3 and JRA-55.

The maps showing RMSEs mimic the maps illustrating the differences between all datasets and the reference dataset GPCPv2.3. The maps with RMSEs between JRA-55 and GPCPv2.3 as well as between the NCEP/DOE R2 and GPCPv2.3 display wide latitudinal bands, with RMSEs between 5–10 mm/day around 5° north. The RMSEs between ERA-5 and GPCPv2.3 and between NCEP/CFSv2 and GPCPv2.3 show thinner bands and slightly lower RMSEs between 3–5 mm/day at 5° north. The grid cells displaying high differences between MERRA-2 and GPCPv2.3 in Figure 2 also depict high RMSEs between MERRA-2 and GPCPv2.3. As expected, the highest three RMSEs are observed for the same cells as before on New Guinea and over Columbia. The highest RMSE, 29.737 mm/day, is found for the same grid cell on New Guinea that showed the highest difference. Other areas showing high RMSEs between MERRA-2 and GPCPv2.3 again include the Atlantic coast of Central Africa, the East African Rift Valley, the Himalayas, and the Tibetan Plateau, and generally the Malay Archipelago. The RMSEs between MERRA-2 and GPCPv2.3 are comparatively small over the ocean; however, at 5° north latitude, we can see a band of elevated RMSEs between 2–4.5 mm/day. As mentioned before, this band is also present in the RMSEs between the other datasets and GPCPv2.3. The RMSEs between NCEP/NCAR R1 and GPCPv2.3 in this band are with 4–7 mm/day higher than the RMSEs between MERRA-2 and GPCPv2.3. With RMSEs between 2–4.5 mm/day, the band at 5° north between NCEP/CFSv2 and GPCPv2.3 looks very similar to the band of RMSEs between MERRA-2 and GPCPv2.3. Examining the RMSEs between NCEP/CFSv2 and GPCPv2.3, we see individual grid cells with higher RMSEs, for example, on the Malay Archipelago, south of the Himalayas, and over Central America. The highest RMSE, 9.109 mm/day, is found over Columbia. Much higher RMSEs can be detected between NCEP/DOE R2 and GPCPv2.3. Three grid cells over Costa Rica and Panama show RMSEs of greater than 16 mm/day. Other areas with high RMSEs include southern India, Sri Lanka, and the region between India and the Maldives, and as well as Indonesia.

The tabulated mean and maximum RMSEs show the lowest mean RMSE between ERA-5 and GPCPv2.3, followed by MERRA-2. The highest mean RMSE is observed between NCEP/DOE R2 and GPCPv2.3. The highest maximum RMSE can be found between MERRA-2 and GPCPv2.3 and the second highest can be observed between NCEP/DOE R2 and GPCPv2.3. The lowest maximum RMSEs can be observed between NCEP/NCAR R1 and GPCPv2.3, closely followed by NCEP/CFSv2, JRA-55, and ERA-5.

#### 4. Discussion

The first point that shall be discussed here is the reliability of the reference dataset GPCPv2.3. The key limitations of GPCPv2.3 listed in Pendergrass et al. [57] include the existence of residual inter-satellite differences at the boundaries between the areas of coverage of the geo-infrared sensors as well as the potential bias in precipitation estimates resulting from significant drifting of the equator-crossing time of some polar-orbiting satellites during their period of service. Based on global water and energy budgets, it was concluded that GPCPv2.3 underestimates precipitation specifically over the ocean [63]. Furthermore, the spatial resolution of 2.5° restricts the usage of the dataset. As mentioned in the introduction, particularly in high mountainous regions, the terrain is complex, and orographic effects cause high spatiotemporal variability in precipitation [5,6], which cannot adequately be captured given this spatial resolution of the dataset. The monthly temporal

resolution is another limiting factor. For hydrological modeling, even in data-scarce regions, the precipitation data are used in at least daily resolution [64].

Despite its limitations, GPCPv2.3 has been used as a reference dataset in many studies such as those of Beniche et al. [65], Anochi et al. [66], Sharma et al. [67], Nogueira [68], Li et al. [69], and Hassler and Lauer [70]. In the study by Beniche et al. [65], precipitation data from GPCPv2.3 were used to evaluate the impacts of El Niño Southern Oscillation events on precipitation over North America and the Pacific. In that by Anochi et al. [66], the GPCPv2.3 dataset was employed as a target with which to train machine learning models and to validate precipitation forecasts for South America. The GPCP precipitation dataset was used as ground truth for correcting Indian Summer Monsoon Rainfall as simulated by the Indian Institute of Tropical Meteorology climate forecast system over the Indian subcontinent [67]. In Nogueira [68], GPCPv2.3 was the reference used to evaluate the performance of ERA-5 and ERA-Interim precipitation worldwide.

From the studies in which GPCPv2.3 was used as a reference dataset, the results from Li et al. [69] and Hassler and Lauer [70] are most comparable to the ones of the present study.

Li et al. [69] evaluated among other things the performance of precipitation data from ERA-5, JRA-55, MERRA-2, and the CFSR against GPCPv2.3. Looking at the time period from 1980 through 2018, they found that all datasets except MERRA-2 show wet biases in precipitation over tropical regions, particularly over the Pacific and Atlantic region of the Intertropical Convergence Zone (ITCZ). Similar to the maps from the correlation analyses presented in this study, their maps depicting calculated correlation coefficients between the annual precipitation anomalies in the different precipitation datasets and GPCPv2.3 annual precipitation anomalies show areas of no correlation for the eastern (dry region) boundaries of the Pacific and Atlantic ocean basins.

In the study by Hassler and Lauer [70], GPCPv2.3 was compared with 10 other precipitation datasets, of which 6 were from reanalyses and 4 were from observational datasets. The comparison focused on the Tropics, the Pacific ITCZ, Central Europe, and the South Asian Monsoon region for the time period from 1983 through 2016. Similar to the results of this study, they found that ERA-5 for the most part agrees better with GPCPv2.3 than MERRA-2 and JRA-55. As in the present study, a strong overestimation of tropical precipitation was found particularly for JRA-55 (especially over the ocean) but also for MERRA-2 (especially over land) and to a lesser extent for ERA-5.

In an older study from Quartly et al. [71], correlation coefficients between GPCPv2 and NCEP/NCAR R1 as well as between GPCPv2 and NCEP/DOE R2 were calculated for the period from 1979 to 2000. The study focused on the ocean and found generally lower correlations between NCEP/DOE R2 and GPCPv2. Quartly et al. [71] also detected much higher precipitation in NCEP/DOE R2 over the ocean as compared to NCEP/NCAR R1 and GPCPv2. Looking at the maps depicting Spearman correlation coefficients from the present study, it becomes clear that even though our mean correlation coefficient between NCEP/DOE R2 and GPCPv2.3 is slightly higher, the correlation over the ocean is lower as compared to NCEP/NCAR R1 and GPCPv2.3. The strong overestimation of precipitation in NCEP/DOE R2 is also evident in the present study, especially over the tropical ocean.

As the focus of this study is on providing guidance in the choice of precipitation data, for example, for hydrologic modeling, the following paragraphs provide advice based on the results presented in Section 3. The recommendations made here are valid for the period from January 2019 to December 2023.

Precipitation rates from ERA-5 and JRA-55 showed very small deviations from the reference dataset GPCPv2.3 over Europe and eastern South America. In the absence of ground observational data, the use of precipitation data from both datasets seems acceptable

in these areas. Over Australia, similarly small deviations were found between precipitation rates from ERA-5 and the reference dataset, as well as between NCEP/CFSv2 and the reference dataset. Using precipitation rates from ERA-5 and NCEP/CFSv2 in Australia seems feasible if no ground observational data are available. ERA-5 also performed well over Central and North America in all areas south of 40° north. In the absence of ground observational data, applying precipitation rates from ERA-5 could be an option. Over the North Atlantic and North Pacific Ocean basins that are south of 70° north, precipitation rates from MERRA-2 closely resembled the reference dataset. The same is true over the Indian Ocean basin and western South Pacific and over the extratropical eastern South Pacific and South Atlantic north of 65° south. In these areas, MERRA-2 performed best closely followed by ERA-5. In the case that no ground observational data are available, the use of precipitation data from MERRA-2 is recommended here.

For many regions with sparse precipitation, high percentage errors between the different datasets and the reference dataset were found. Therefore, replacing ground observational data with precipitation rates from the datasets presented here is generally not recommended. These regions include the Tibetan Plateau, parts of Central Asia, southern Patagonia, the Atacama desert, the Sahara desert and the Sahel, western Greenland, East Antarctica, and the oceanic regions of sparse precipitation along the west coasts of southern Africa and of South America. As the absence of ground observational data in many of these regions may force researchers to find alternative data sources, I will list for each of these regions which precipitation dataset performed better than the others (although not performing well).

Over the Tibetan Plateau and Central Asia, precipitation rates from ERA-5 and NCEP/DOE R2 showed the smallest (but still considerable) deviations from the reference dataset. Over southern Patagonia, NCEP/NCAR R1 and NCEP/DOE R2 performed better than the other datasets. Precipitation rates over the Atacama desert were comparatively satisfactorily represented by ERA-5 and JRA-55. Over the Sahara desert and the Sahel, precipitation rates from ERA-5 showed the smallest deviations from the reference dataset. Over western Greenland and East Antarctica, JRA-55 and NCEP/DOE R2 performed better than the other datasets. Compared to the other datasets, NCEP/NCAR R1 satisfactorily represented precipitation rates over the oceanic region along the west coast of southern Africa. The same is true for JRA-55 over the oceanic region along the west coast of South America.

## 5. Conclusions

Particularly in data-sparse regions, it is tempting to use precipitation rates from reanalysis datasets in hydrologic modeling. However, it needs to be taken into account that the reliability of reanalysis data varies in time and space and differs according to climate variables. Precipitation rates are among the more uncertain variables in reanalysis datasets, especially in the first generation of global reanalyses such as NCEP/NCAR R1. It is advisable to check for the limitations of precipitation data, especially from reanalysis datasets, prior to their application. In this study, precipitation rates from the reanalysis datasets ERA-5, JRA-55, MERRA-2, NCEP/NCAR R1, NCEP/DOE R2, and the analysis dataset NCEP/CFSv2 were compared with precipitation data from the merged satellite and rain gauge dataset GPCPv2.3 over the period from 2019 to 2023.

Overall, the precipitation rates from ERA-5 agreed best with the GPCPv2.3 reference precipitation data: the smallest mean and maximum percentage errors, the highest mean correlation, and the smallest mean RMSE were found for ERA-5. ERA-5 performed well over Europe, Australia, and southern North America. However, even though the performance of ERA-5 can be considered the best overall, there are still regions in which the

application of precipitation rates from ERA-5 cannot be recommended. These regions include the Tibetan plateau and parts of Central Asia, western Greenland and East Antarctica, the Atacama desert, southern Patagonia, the Sahara desert and the Sahel, and the oceanic regions with sparse precipitation along the west coasts of South America and southern Africa. It shall be mentioned here that even though ERA-5 showed considerable deviations from the reference dataset in the above-mentioned regions, it still performed better than the other datasets over the Sahara desert and the Sahel, as well as over the Atacama desert, the Tibetan Plateau, and Central Asia.

JRA-55, MERRA-2, and NCEP/CFSv2 all performed well over the eastern part of North America and Europe. MERRA-2 also performed well over the Indian Ocean basin, and NCEP/CFSv2 exhibited good agreement with the reference dataset over Australia. However, these three datasets performed poorly in several other regions. JRA-55 overestimated precipitation over the tropical ocean, and MERRA-2 did so over tropical land regions. NCEP/CFSv2 overestimated precipitation in different geographical regions over land including the Malay Archipelago, the region south of the Himalayas, and southern Patagonia.

Even though NCEP/NCAR R1 showed the smallest mean differences from the reference dataset and therefore also the closest value for mean total global precipitation, the use of precipitation rates from NCEP/NCAR R1 generally cannot be recommended. Precipitation rates from NCEP/NCAR R1 showed the highest mean and by far the highest maximum percentage errors as well as the lowest correlations with GPCPv2.3. The precipitation rates from NCEP/DOE R2 were significantly higher than the reference dataset, and their usage is also not recommended. Precipitation rates from NCEP/DOE R2 exhibited the second lowest correlations with precipitation rates from GPCPv2.3 and the highest mean RMSE.

**Funding:** This research received no external funding.

**Data Availability Statement:** The data presented in this study are openly available on the following websites: ERA-5 <https://cds.climate.copernicus.eu/datasets/reanalysis-era5-single-levels-monthly-means> (accessed on 1 December 2024); JRA-55 <https://rda.ucar.edu/datasets/d628001/> (accessed on 1 December 2024); MERRA-2 [https://disc.gsfc.nasa.gov/datasets/M2TMNXAER\\_5.12.4/summary](https://disc.gsfc.nasa.gov/datasets/M2TMNXAER_5.12.4/summary) (accessed on 1 December 2024); NCEP/NCAR R1 <https://psl.noaa.gov/data/gridded/data.ncep.reanalysis.html> (accessed on 1 December 2024); NCEP/DOE R2 <https://psl.noaa.gov/data/gridded/data.ncep.reanalysis2.html> (accessed on 1 December 2024); NCEP/CFSv2 <https://rda.ucar.edu/datasets/d094002> (accessed on 1 December 2024); and GPCPv2.3 <https://psl.noaa.gov/data/gridded/data.gpcp.html> (accessed on 1 December 2024).

**Conflicts of Interest:** The author declares no conflict of interest.

## References

1. Monfray, P.; Bley, D. JPI Climate: A Key Player in Advancing Climate Services in Europe. *Clim. Serv.* **2016**, *4*, 61–64. [[CrossRef](#)]
2. Dos Reis, A.A.; Weerts, A.; Ramos, M.H.; Wetterhall, F.; dos S. Fernandes, W. Hydrological Data and Modeling to Combine and Validate Precipitation Datasets Relevant to Hydrological Applications. *J. Hydrol. Reg. Stud.* **2022**, *44*, 101200. [[CrossRef](#)]
3. Zhou, L.; Koike, T.; Takeuchi, K.; Rasmy, M.; Onuma, K.; Ito, H.; Selvarajah, H.; Liu, L.; Li, X.; Ao, T. A Study on Availability of Ground Observations and Its Impacts on Bias Correction of Satellite Precipitation Products and Hydrologic Simulation Efficiency. *J. Hydrol.* **2022**, *610*, 127595. [[CrossRef](#)]
4. Tapiador, F.J.; Navarro, A.; Levizzani, V.; García-Ortega, E.; Huffman, G.J.; Kidd, C.; Kucera, P.A.; Kummerow, C.D.; Masunaga, H.; Petersen, W.A.; et al. Global Precipitation Measurements for Validating Climate Models. *Atmos. Res.* **2017**, *197*, 1–20. [[CrossRef](#)]
5. Houze, R.A. Orographic Effects on Precipitating Clouds. *Rev. Geophys.* **2012**, *50*, 1–47. [[CrossRef](#)]
6. Strauch, M.; Kumar, R.; Eisner, S.; Mulligan, M.; Reinhardt, J.; Santini, W.; Vetter, T.; Friesen, J. Adjustment of Global Precipitation Data for Enhanced Hydrologic Modeling of Tropical Andean Watersheds. *Clim. Change* **2017**, *141*, 547–560. [[CrossRef](#)]

7. Krysanova, V.; Wortmann, M.; Bolch, T.; Merz, B.; Duethmann, D.; Walter, J.; Huang, S.; Tong, J.; Buda, S.; Kundzewicz, Z.W. Analysis of current trends in climate parameters, river discharge and glaciers in the Aksu River basin (Central Asia). *Hydrol. Sci. J.* **2015**, *60*, 566–590. [[CrossRef](#)]
8. Wortmann, M.; Bolch, T.; Menz, C.; Tong, J.; Krysanova, V. Comparison and Correction of High-Mountain Precipitation Data Based on Glacio-Hydrological Modeling in the Tarim River Headwaters (High Asia). *J. Hydrometeorol.* **2018**, *19*, 777–801. [[CrossRef](#)]
9. Li, H.; Haugen, J.E.; Xu, C.Y. Precipitation Pattern in the Western Himalayas Revealed by Four Datasets. *Hydrol. Earth Syst. Sci.* **2018**, *22*, 5097–5110. [[CrossRef](#)]
10. Bisht, D.S.; Chowdhury, B.; Rawat, S.S.; Pottakkal, J.G. Performance Ranking of Global Precipitation Estimates over Data Scarce Western Himalayan Region of India. *Theor. Appl. Clim.* **2024**, *155*, 7515–7537. [[CrossRef](#)]
11. Hamal, K.; Sharma, S.; Khadka, N.; Baniya, B.; Ali, M.; Shrestha, M.S.; Xu, T.; Shrestha, D.; Dawadi, B. Evaluation of MERRA-2 Precipitation Products Using Gauge Observation in Nepal. *Hydrology* **2020**, *7*, 40. [[CrossRef](#)]
12. Bai, P.; Liu, X. Evaluation of Five Satellite-Based Precipitation Products in Two Gauge-Scarce Basins on the Tibetan Plateau. *Remote Sens.* **2018**, *10*, 1316. [[CrossRef](#)]
13. Liu, Z.; Yang, Q.; Shao, J.; Wang, G.; Liu, H.; Tang, X.; Xue, Y.; Bai, L. Improving Daily Precipitation Estimation in the Data Scarce Area by Merging Rain Gauge and TRMM Data with a Transfer Learning Framework. *J. Hydrol.* **2022**, *613*, 128455. [[CrossRef](#)]
14. Condom, T.; Martínez, R.; Pabón, J.D.; Costa, F.; Pineda, L.; Nieto, J.J.; López, F.; Villacis, M. Climatological and Hydrological Observations for the South American Andes: In Situ Stations, Satellite, and Reanalysis Data Sets. *Front Earth Sci.* **2020**, *8*, 92. [[CrossRef](#)]
15. Rhoujjati, N.; Ait Brahim, Y.; Hanich, L.; Rhoujjati, A.; Patris, N.; Chehbouni, A.; Bouchaou, L. Precipitation Isotopes to Elucidate Moisture Sources in the Western Mediterranean: Case of the Middle Atlas Mountains, Morocco. *Environ. Earth Sci.* **2023**, *82*, 250. [[CrossRef](#)]
16. Hanich, L.; Chehbouni, A.; Gascoin, S.; Boudhar, A.; Jarlan, L.; Trambly, Y.; Boulet, G.; Marchane, A.; Baba, M.W.; Kinnard, C.; et al. Snow Hydrology in the Moroccan Atlas Mountains. *J. Hydrol. Reg. Stud.* **2022**, *42*, 101101. [[CrossRef](#)]
17. Gebere, S.B.; Alamirew, T.; Merkel, B.J.; Melesse, A.M. Performance of High Resolution Satellite Rainfall Products over Data Scarce Parts of Eastern Ethiopia. *Remote Sens.* **2015**, *7*, 11639–11663. [[CrossRef](#)]
18. European Centre for Medium-Range Weather Forecasts (ECMWF). Fact Sheet: Reanalysis. ECMWF. Available online: <https://www.ecmwf.int/en/about/media-centre/focus/2023/fact-sheet-reanalysis> (accessed on 1 December 2024).
19. Hersbach, H.; Bell, B.; Berrisford, P.; Hirahara, S.; Horányi, A.; Muñoz-Sabater, J.; Nicolas, J.; Peubey, C.; Radu, R.; Schepers, D.; et al. The ERA5 Global Reanalysis. *Q. J. R. Meteorol. Soc.* **2020**, *146*, 1999–2049. [[CrossRef](#)]
20. Bengtsson, L.; Kanamitsu, M.; Källberg, P.; Uppala, S. FGGE Research Activities at ECMWF. *Bull. Am. Meteorol. Soc.* **1982**, *63*, 277–303. [[CrossRef](#)]
21. Ploshay, J.J.; White, R.; Miyakoda, K. *FGGE Level III-b Daily Global Analyses, Part I*; NOAA Data Report ERL GFDL-1; U.S. Dept. of Commerce, National Oceanic and Atmospheric Administration, Environmental Research Laboratories, Geophysical Fluid Dynamics Laboratory: Princeton, NJ, USA, 1983.
22. Kalnay, E.; Kanamitsu, M.; Kistler, R.; Collins, W.; Deaven, D.; Gandin, L.; Iredell, M.; Saha, S.; White, G.; Woollen, J.; et al. The NCEP/NCAR 40-Year Reanalysis Project. *Bull. Am. Meteorol. Soc.* **1996**, *77*, 437–472. [[CrossRef](#)]
23. Gibson, J.K.; Källberg, P.; Uppala, S.; Hernandez, A.; Nomura, A.; Serrano, E. *ECMWF Re-Analysis Project Report Series 1. ERA-15 Description*; ECMWF Re-Analysis Project Report Series; U.S. Dept. of Commerce, National Oceanic and Atmospheric Administration, Environmental Research Laboratories, Geophysical Fluid Dynamics Laboratory: Princeton, NJ, USA, 1999.
24. Compo, G.P.; Whitaker, J.S.; Sardeshmukh, P.D.; Matsui, N.; Allan, R.J.; Yin, X.; Gleason, B.E.; Vose, R.S.; Rutledge, G.; Bessemoulin, P.; et al. The Twentieth Century Reanalysis Project. *Q. J. R. Meteorol. Soc.* **2011**, *137*, 1–28. [[CrossRef](#)]
25. Thorne, P.W.; Vose, R.S. Reanalyses Suitable for Characterizing Long-Term Trends. *Bull. Am. Meteorol. Soc.* **2010**, *91*, 353–361. [[CrossRef](#)]
26. Hoffman, R.N.; Privé, N.; Bourassa, M. Comments on “Reanalyses and Observations: What’s the Difference?”. *Bull. Am. Meteorol. Soc.* **2017**, *98*, 2455–2459. [[CrossRef](#)]
27. Kistler, R.; Kalnay, E.; Collins, W.; Saha, S.; White, G.; Woollen, J.; Chelliah, M.; Ebisuzaki, W.; Kanamitsu, M.; Kousky, V.; et al. The NCEP–NCAR 50-Year Reanalysis: Monthly Means CD-ROM and Documentation. *Bull. Am. Meteorol. Soc.* **2001**, *82*, 247–268. [[CrossRef](#)]
28. Gelaro, R.; McCarty, W.; Suárez, M.J.; Todling, R.; Molod, A.; Takacs, L.; Randles, C.A.; Darmenov, A.; Bosilovich, M.G.; Reichle, R.; et al. The Modern-Era Retrospective Analysis for Research and Applications, Version 2 (MERRA-2). *J. Clim.* **2017**, *30*, 5419–5454. [[CrossRef](#)] [[PubMed](#)]
29. Reichle, R.H.; Liu, Q.; Koster, R.D.; Draper, C.S.; Mahanama, S.P.P.; Partyka, G.S. Land Surface Precipitation in MERRA-2. *J. Clim.* **2017**, *30*, 1643–1664. [[CrossRef](#)]
30. Parker, W.S. Reanalyses and Observations: What’s the Difference? *Bull. Am Meteorol. Soc.* **2016**, *97*, 1565–1572. [[CrossRef](#)]

31. European Centre for Medium-Range Weather Forecasts (ECMWF). ERA5: Data Documentation. Available online: <https://confluence.ecmwf.int/display/CKB/ERA5:+data+documentation> (accessed on 1 December 2024).
32. Hersbach, H.; Bell, B.; Berrisford, P.; Biavati, G.; Horányi, A.; Muñoz Sabater, J.; Nicolas, J.; Peubey, C.; Radu, R.; Rozum, I.; et al. ERA5 Monthly Averaged Data on Single Levels from 1940 to Present. Available online: <https://cds.climate.copernicus.eu/datasets/reanalysis-era5-single-levels-monthly-means> (accessed on 1 December 2024).
33. Hersbach, H.; National Center for Atmospheric Research Staff (Eds.) The Climate Data Guide: ERA5 Atmospheric Reanalysis. Available online: <https://climatedataguide.ucar.edu/climate-data/era5-atmospheric-reanalysis> (accessed on 1 December 2024).
34. Kobayashi, S.; Ota, Y.; Harada, Y.; Ebata, A.; Moriya, M.; Onoda, H.; Onogi, K.; Kamahori, H.; Kobayashi, C.; Endo, H.; et al. The JRA-55 Reanalysis: General Specifications and Basic Characteristics. *J. Meteorol. Soc. Jpn.* **2015**, *93*, 5–48. [[CrossRef](#)]
35. Harada, Y.; Kamahori, H.; Kobayashi, C.; Endo, H.; Kobayashi, S.; Ota, Y.; Onoda, H.; Onogi, K.; Miyaoka, K.; Takahashi, K. The JRA-55 Reanalysis: Representation of Atmospheric Circulation and Climate Variability. *J. Meteorol. Soc. Jpn.* **2016**, *94*, 269–302. [[CrossRef](#)]
36. Japan Meteorological Agency (JMA). *JRA-55 Product Users' Handbook Model Grid Data*; Japan Meteorological Agency: Tokyo, Japan, 2014.
37. Japan Meteorological Agency/Japan JRA-55: Japanese 55-Year Reanalysis, Monthly Means and Variances. Available online: <https://rda.ucar.edu/datasets/d628001/> (accessed on 1 December 2024).
38. Kobayashi, S.; National Center for Atmospheric Research Staff (Eds.) The Climate Data Guide: JRA-55. Available online: <https://climatedataguide.ucar.edu/climate-data/jra-55> (accessed on 1 December 2024).
39. Molod, A.; Takacs, L.; Suarez, M.; Bacmeister, J. Development of the GEOS-5 Atmospheric General Circulation Model: Evolution from MERRA to MERRA2. *Geosci. Model. Dev.* **2015**, *8*, 1339–1356. [[CrossRef](#)]
40. Global Modeling and Assimilation Office (GMAO). MERRA-2 TavGM\_2d\_aer\_Nx: 2d, Monthly Mean, Time-Averaged, Single-Level, Assimilation, Aerosol Diagnostics V5.12.4. Available online: [https://disc.gsfc.nasa.gov/datasets/M2TMNXAER\\_5.12.4/summary](https://disc.gsfc.nasa.gov/datasets/M2TMNXAER_5.12.4/summary) (accessed on 1 December 2024).
41. Koninklijk Nederlands Meteorologisch Instituut (KNMI); World Meteorological Organization (WMO). Climate Explorer: Starting Point. Available online: <https://climexp.knmi.nl/start.cgi> (accessed on 1 December 2024).
42. Bosilovich, M.; Cullather, R.; National Center for Atmospheric Research Staff (Eds.) The Climate Data Guide: NASA's MERRA2 Reanalysis. Available online: <https://climatedataguide.ucar.edu/climate-data/nasas-merra2-reanalysis> (accessed on 1 December 2024).
43. Physical Sciences Laboratory (PSL) of the National Oceanic and Atmospheric Administration (NOAA). NCEP-NCAR Reanalysis 1. Available online: <https://psl.noaa.gov/data/gridded/data.ncep.reanalysis.html> (accessed on 1 December 2024).
44. Kanamitsu, M.; Ebisuzaki, W.; Woollen, J.; Yang, S.-K.; Hnilo, J.J.; Fiorino, M.; Potter, G.L. NCEP–DOE AMIP-II Reanalysis (R-2). *Bull. Am. Meteorol. Soc.* **2002**, *83*, 1631–1644. [[CrossRef](#)]
45. Xie, P.; Arkin, P.A. Global Precipitation: A 17-Year Monthly Analysis Based on Gauge Observations, Satellite Estimates, and Numerical Model Outputs. *Bull. Am. Meteorol. Soc.* **1997**, *78*, 2539–2558. [[CrossRef](#)]
46. Physical Sciences Laboratory (PSL) of the National Oceanic and Atmospheric Administration (NOAA) NCEP/DOE Reanalysis II. Available online: <https://psl.noaa.gov/data/gridded/data.ncep.reanalysis2.html> (accessed on 1 December 2024).
47. Saha, S.; Moorthi, S.; Wu, X.; Wang, J.; Nadiga, S.; Tripp, P.; Behringer, D.; Hou, Y.T.; Chuang, H.Y.; Iredell, M.; et al. The NCEP Climate Forecast System Version 2. *J. Clim.* **2014**, *27*, 2185–2208. [[CrossRef](#)]
48. Saha, S.; Moorthi, S.; Pan, H.L.; Wu, X.; Wang, J.; Nadiga, S.; Tripp, P.; Kistler, R.; Woollen, J.; Behringer, D.; et al. The NCEP Climate Forecast System Reanalysis. *Bull. Am. Meteorol. Soc.* **2010**, *91*, 1015–1057. [[CrossRef](#)]
49. Saha, S.; Nadiga, S.; Thiaw, C.; Wang, J.; Wang, W.; Zhang, Q.; Van den Dool, H.M.; Pan, H.-L.; Moorthi, S.; Behringer, D.; et al. The NCEP Climate Forecast System. *J. Clim.* **2006**, *19*, 3483–3517. [[CrossRef](#)]
50. Kleist, D.; Carley, J.R.; Collard, A.; Liu, E.; Liu, S.; Martin, C.R.; Thomas, C.; Treadon, R.; Vernieres, G. *Current State of Data Assimilation Capabilities at NCEP's Modeling Center*; Office note (NCEP (U.S.) 514; U.S. Dept. of Commerce, National Oceanic and Atmospheric Administration, National Weather Service, National Centers for Environmental Prediction: College Park, MD, USA, 2023).
51. McClung, T. *CFSv2\_Documentation\_TIN\_Amend\_10-55\_CFS\_031511*, Technical Implementation Notice 10-55, Amended. 2011.
52. Saha, S.; Moorthi, S.; Wu, X.; Wang, J.; Nadiga, S.; Tripp, P.; Behringer, D.; Hou, Y.-T.; Chuang, H.; Iredell, M.; et al. NCEP Climate Forecast System Version 2 (CFSv2) Monthly Products. Available online: <https://rda.ucar.edu/datasets/d094002/> (accessed on 1 December 2024).
53. Huffman, G.J.; Adler, R.F.; Arkin, P.; Chang, A.; Ferraro, R.; Gruber, A.; Janowiak, J.; McNab, A.; Rudolf, B.; Schneider, U. The Global Precipitation Climatology Project (GPCP) Combined Precipitation Dataset. *Bull. Am. Meteorol. Soc.* **1997**, *78*, 5–20. [[CrossRef](#)]
54. Arkin, P.A.; Xie, P. The Global Precipitation Climatology Project: First Algorithm Intercomparison Project. *Bull. Am. Meteorol. Soc.* **1994**, *75*, 401–420. [[CrossRef](#)]

55. Huffman, G.J.; Adler, R.F.; Rudolf, B.; Schneider, U.; Keehn, P.R. Global Precipitation Estimates Based on a Technique for Combining Satellite-Based Estimates, Rain Gauge Analysis, and NWP Model Precipitation Information. *J. Clim.* **1995**, *8*, 1284–1295. [[CrossRef](#)]
56. Adler, R.F.; Sapiano, M.R.P.; Huffman, G.J.; Wang, J.J.; Gu, G.; Bolvin, D.; Chiu, L.; Schneider, U.; Becker, A.; Nelkin, E.; et al. The Global Precipitation Climatology Project (GPCP) Monthly Analysis (New Version 2.3) and a Review of 2017 Global Precipitation. *Atmosphere* **2018**, *9*, 138. [[CrossRef](#)] [[PubMed](#)]
57. Pendergrass, A.; Wang, J.-J.; National Center for Atmospheric Research Staff (Eds.) The Climate Data Guide: GPCP (Monthly): Global Precipitation Climatology Project. Available online: <https://climatedataguide.ucar.edu/climate-data/gpcp-monthly-global-precipitation-climatology-project> (accessed on 2 December 2024).
58. Gu, G.; Adler, R.F. Variability and Trends in Tropical Precipitation Intensity in Observations and Climate Models. *Clim. Dyn.* **2024**, *62*, 7429–7443. [[CrossRef](#)]
59. Physical Sciences Laboratory (PSL) of the National Oceanic and Atmospheric Administration (NOAA) Global Precipitation Climatology Project (GPCP) Monthly Analysis Product. Available online: <https://psl.noaa.gov/data/gridded/data.gpcp.html> (accessed on 1 December 2024).
60. Fiorino, M. *NMC GrADS User-Defined Function 1: Regrid*; Development Division, National Meteorological Center: Washington, DC, USA, 1993.
61. Lohninger, H. *Teach/Me-Data Analysis*; Springer: Berlin, Germany, 1999.
62. Chai, T.; Draxler, R.R. Root Mean Square Error (RMSE) or Mean Absolute Error (MAE)? -Arguments against Avoiding RMSE in the Literature. *Geosci. Model. Dev.* **2014**, *7*, 1247–1250. [[CrossRef](#)]
63. Huffman, G.J.; Adler, R.F.; Behrangi, A.; Bolvin, D.T.; Nelkin, E.J.; Guojun, G.U.; Ehsani, M.R. The New Version 3.2 Global Precipitation Climatology Project (GPCP) Monthly and Daily Precipitation Products. *J. Clim.* **2023**, *36*, 7635–7655. [[CrossRef](#)]
64. Zhou, J.; Wang, X.; Ma, J.; Jia, Z.; Wang, X.; Zhang, X.; Feng, X.; Sun, Z.; Tu, Y.; Yao, W. An Approach to Select Optimum Inputs for Hydrological Modeling to Improve Simulation Accuracy in Data-Scarce Regions. *J. Hydrol. Reg. Stud.* **2023**, *47*, 101447. [[CrossRef](#)]
65. Beniche, M.; Vialard, J.; Lengaigne, M.; Voldoire, A.; Srinivas, G.; Hall, N.M.J. A Distinct and Reproducible Teleconnection Pattern over North America during Extreme El Niño Events. *Sci. Rep.* **2024**, *14*, 2457. [[CrossRef](#)]
66. Anochi, J.A.; de Almeida, V.A.; de Campos Velho, H.F. Machine Learning for Climate Precipitation Prediction Modeling over South America. *Remote Sens.* **2021**, *13*, 2468. [[CrossRef](#)]
67. Sharma, S.C.M.; Kumar, B.; Mitra, A.; Saha, S.K. Deep Learning-Based Bias Correction of ISMR Simulated by GCM. *Atmos. Res.* **2024**, *309*, 107589. [[CrossRef](#)]
68. Nogueira, M. Inter-Comparison of ERA-5, ERA-Interim and GPCP Rainfall over the Last 40 Years: Process-Based Analysis of Systematic and Random Differences. *J. Hydrol.* **2020**, *583*, 124632. [[CrossRef](#)]
69. Li, C.; Zhao, T.; Shi, C.; Liu, Z. Assessment of Precipitation from the CRA40 Dataset and New Generation Reanalysis Datasets in the Global Domain. *Int. J. Climatol.* **2021**, *41*, 5243–5263. [[CrossRef](#)]
70. Hassler, B.; Lauer, A. Comparison of Reanalysis and Observational Precipitation Datasets Including Era5 and Wfde5. *Atmosphere* **2021**, *12*, 1462. [[CrossRef](#)]
71. Quartly, G.D.; Kyte, E.A.; Srokosz, M.A.; Tsimplis, M.N. An Intercomparison of Global Oceanic Precipitation Climatologies. *J. Geophys. Res. Atmos.* **2007**, *112*, D10. [[CrossRef](#)]

**Disclaimer/Publisher’s Note:** The statements, opinions and data contained in all publications are solely those of the individual author(s) and contributor(s) and not of MDPI and/or the editor(s). MDPI and/or the editor(s) disclaim responsibility for any injury to people or property resulting from any ideas, methods, instructions or products referred to in the content.